# Differential cross section for electron impact excitation of metastable helium

Arthur G. Zajonc,* Gabriel Weinreich, John C. Pearl†, and Jens C. Zorn
*Randall Laboratory of Physics, University of Michigan, Ann Arbor, Michigan 48109*
(Received 2 September 1977)

By analyzing the time-of-flight distribution of metastable helium atoms produced by bombardment of a ground-state atomic beam by low-energy electrons, we have measured the differential cross section for excitation of the $2^3S_1$ state over the energy range 19.9–20.4 eV. The results are compared with those determined from electron energy-loss experiments as well as with various theoretical predictions.

## I. INTRODUCTION

Because of the ease of helium-beam production and its relative simplicity as an atomic system for theoretical study, electron-helium collisions have long been the subject of active experimental and theoretical investigation. An extra impetus was received from the discovery in the early sixties of resonant structure in cross-section measurements.

Various techniques have been used to measure the total cross section[1-3] and the total metastable production[4-6] ($2\,^3S+2\,^1S$) for electron excitation of helium. The excitation cross section at selected angles has been measured by Ehrhardt and coworkers[7,8] and more recently by Andrick, Langhans, Linder, and Seng[9] and by Pichou, Huetz, Joyez, Landau, and Mazeau.[10] A comprehensive review of this work through 1972 has been given by Schulz.[11]

Theoretical calculations of the differential cross section have been performed by several groups, notably Burke, Cooper, and Ormonde,[12] using a close-coupling technique, and Oberoi and Nesbet,[13] who used a variational technique. More recently, Nesbet[14] has calculated cross sections near threshold and Sinfailam[15] has used an $R$-matrix method to calculate elastic and inelastic cross sections for electron energies from 19.5 to 22.0 eV.

The present experiment differs from previous measurements in that the differential cross section is calculated from metastable-atom time-of-flight (MTOF) distributions.[16] By detecting the metastable atom, we circumvent a number of difficulties[10] inherent in energy analysis of low-energy electrons.

## II. EXPERIMENTAL PROCEDURE AND APPARATUS

Figure 1 shows the overall layout of our apparatus, which is a modification of the one used by Heppner and Zorn.[17] The vacuum system consists of differentially pumped source and detection chambers. The atomic beam originates in a source cell, is collimated, and intersects a pulsed electron beam where a small fraction of the ground-state beam is excited to the $2\,^3S_1$ metastable state. The metastable beam then exits through a slit in the interaction region of the electron gun and is again collimated before detection. The resulting signal is amplified, time-to-height converted, and fed into a multichannel analyzer for storage and display. The data from each good run are transferred to a computer.

Helium effuses from the room-temperature source cell through a circular orifice of 0.13-mm diameter. The source-cell pressure is monitored by a Barocell variable-capacitance electronic ma-

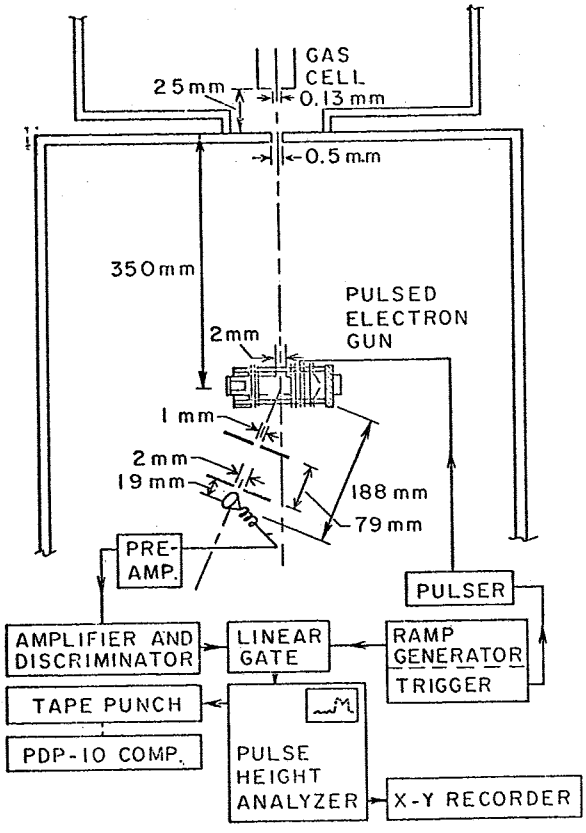


FIG. 1. Overall layout of the experiment and block diagram of the electronics.

nometer and is typically in the range of 1 torr. In this range of pressure, temperature, and orifice diameter, no appreciable deviations from the Maxwell velocity distribution are expected and, indeed, in the subsequent analysis of the time-of-flight distributions no indication of such deviations was found.

The electron gun consists of a Phillips type-M cathode mounted into a molybdenum heat shield which is, in turn, mounted in a boron nitride base. A Pierce shield and accelerating electrode focus and accelerate the electrons into an einzel lens which further focuses the electron beam into the interaction region. Electrons transmitted through the interaction region are accelerated into a Faraday cup where they are trapped. All components which are exposed to the electron beam are fabricated from molybdenum. Accurate reproducible location of all components is achieved through the use of lapped ground-glass locating rods that are press fit into a stainless-steel end block. Electrode spacing is maintained with mica sheets. Details can be found in Ref. 18.

Typical operating voltages with respect to the cathode were: Pierce shield, −2 V; accelerating electrode, 22 V; einzel-lens electrodes, 18, 14, and 19.5 V. The post-interaction-region voltages were kept moderately high (~30 V) to reduce backscattering. The current to the Faraday cup under such conditions is about 500 nA. For time-of-flight operation, the middle electrode of the einzel lens is biased negative and then pulsed to its operating voltage for 5 $\mu$sec at a frequency of about 5 kHz. In order to reduce background, the entire electron-gun assembly is floated about 50 V positive with respect to the vacuum chamber and detector housing.

The average kinetic energy of electrons in the interaction region differs from the potential difference between that region and the gun cathode by an amount that we refer to as the "voltage offset." The reason that the voltage offset is not zero lies in the various electrode contact potentials; the situation is further complicated by the gradual buildup of insulating layers and the resulting accumulation of charge which introduces a time dependence into the voltage offset. Our approach to this problem has been to determine both the voltage offset and the distribution of electron energies from a careful analysis of the "appearance-potential curve" for metastable helium. This curve is obtained by operating the gun in an unpulsed mode and flooding the interaction region with helium at low pressure. The interaction-region voltage is then varied from about 19.5 to about 21.5 V and the metastable flux is monitored. A typical appearance-potential curve is shown in Fig. 2. By comparing this curve with the metastable-production curve of Pichanick and Simpson,[5] whose resolution was considerably better than ours, we can find the approximate electron-energy distribution and voltage offset.

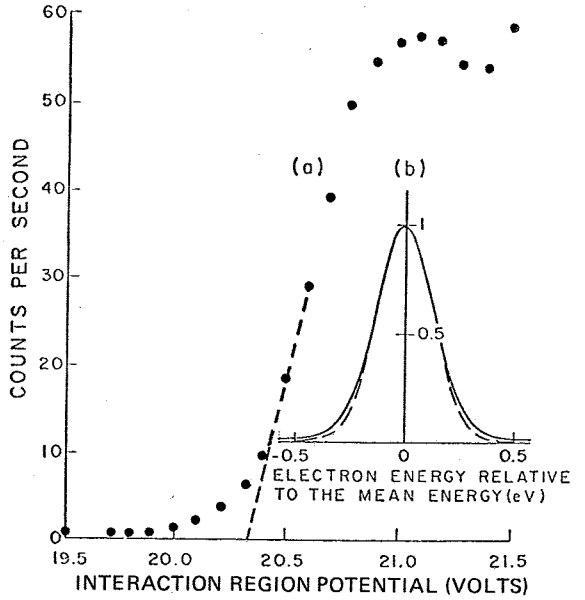


FIG. 2. (a) Typical helium appearance-potential curve. The solid circles are experimental points. The dashed straight line indicates the voltage offset is 0.52 V. (b) Comparison of a Gaussian electron-energy distribution (dashed curve) with the extended Gaussian of Eq. (1) (solid curve); $\Gamma = 0.3$, $a = 0.2$, $b = 0.05$.

We were able to obtain a satisfactory fit of our experimental appearance-potential curve by assuming that the electrons are spread about their mean energy $\epsilon_0$ according to the distribution function

$$f(\epsilon) = \exp\left(\frac{-2.77(\epsilon-\epsilon_0)^2}{\Gamma^2}\right) + \frac{b}{1+(\epsilon-\epsilon_0)^2/a^2}. \qquad (1)$$

A pure Gaussian distribution without the tails added by the second term was not sufficient. Typically, $\Gamma$ varied from 0.2 to 0.4 and $a$ from 0.1 to 0.3. The weighting constant $b$ was typically 0.05. Our electron-energy distribution appears to have, therefore, a full width at half maximum of ~0.25 eV and long tails. This agrees with the findings of Collins *et al.*[19] for a similar electron gun. The high-energy tail of the electron-energy distribution is especially significant near threshold, where the cross section rises sharply with energy.

Although the fitting procedure described above yields the voltage offset, it should be noted that the MTOF spectra themselves are also an excellent indication of that quantity. Since, at a given observation angle $\alpha$, the cutoff momenta for the metastable atoms depend only on the incident-electron energy, the width of the spectrum compared

to the width of the simulated spectrum (see the Appendix) is a measure of the voltage offset.

The metastable-atom detector is a Channeltron continuous electron multiplier[20] which is mounted 18.8-cm downstream from the region of metastable production. It can be pivoted about the interaction region in the plane of scattering and has an angular resolution of 0.5°. The Channeltron signal is preamplified, amplified, and discriminated so that the resulting pulses can be used to gate an accurately generated ramp triggered synchronously with the electron-gun pulse. This process converts the times of flight into pulse heights which are then fed to a Nuclear Data 2200 multichannel analyzer in the pulse-height mode. Accumulation times of 2000 sec and count rates of 2 counts/sec were typical for the MTOF spectra used in this work. Time-base calibration is established by a time-mark generator accurate to 0.2 $\mu$sec, which provides markers at 10-$\mu$sec intervals from 0 to 150 $\mu$sec after the gun pulse.

The almost total absence of background, as illustrated in Figs. 3–5, was achieved by careful shielding and adjustment of the relative potentials of the various parts of the apparatus. Without these precautions, stray charged particles arriving at the detector could easily produce count rates 20 times as large as our signals.

The statistical uncertainties associated with each MTOF distribution ranged from 8% to 16%. Since the cross section was measured both as a function of energy and of scattering angle, uncertainties must be given for each of these quantities. The electron-energy resolution was limited by the electron gun to about 0.25 eV. Since we do not measure the cross section as a function of scattering angle directly, the equivalent uncertainty must be determined from Eq. (A8). It is typically ±7°. Combining statistical and instrumental uncertainties, an overall uncertainty of about 15% must be ascribed to our measured values of the differential cross section.

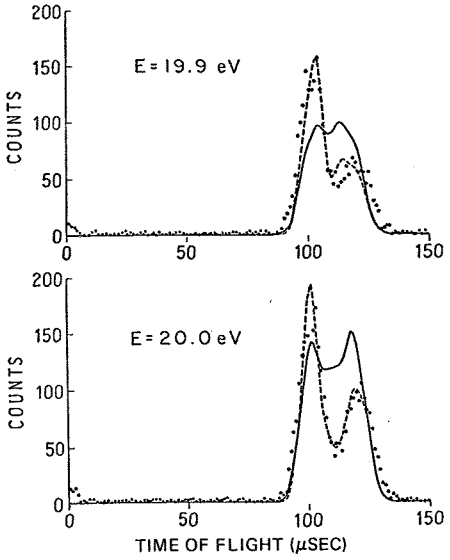


FIG. 3. MTOF distributions at $\alpha = 11.8°$: dots—actual data; dashed curve—simulated distributions using empirical cross sections (see Fig. 6); solid curve—simulated distributions, isotropic cross section using energy variation of Pichanick and Simpson, Ref. 5. The spectra are peak normalized at the 20.3-eV distribution only.

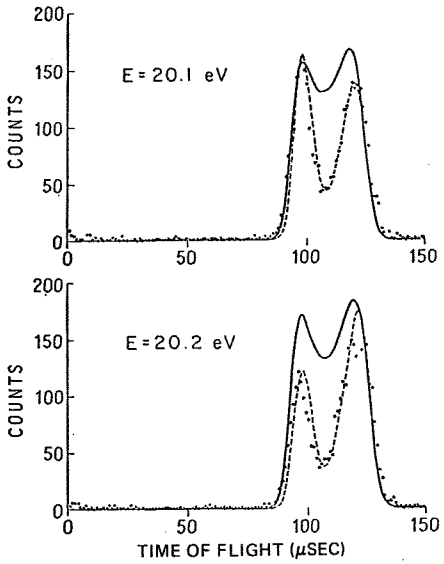


FIG. 4. MTOF distributions at $\alpha = 11.8°$: conditions are the same as in Fig. 2 except for the incident electron energy.

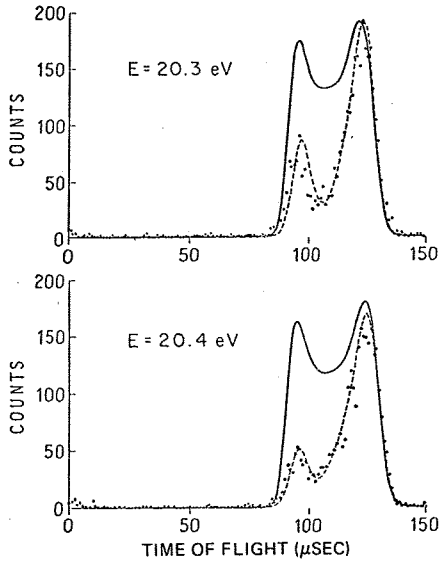


FIG. 5. MTOF distributions at $\alpha = 11.8°$: conditions are the same as in Fig. 2 except for the incident electron energy.

## III. REDUCTION OF DATA

Our method of analysis is based on the discussion of collision kinematics developed in the Appendix. It should be especially emphasized that, in the ideal case of perfect geometrical resolution and of a perfectly monochromatic electron beam, there would be (for a given detector position) a one-to-one correspondence between the metastable-atom time-of-flight and the angle $\theta$ through which the electron is scattered.

We utilized the results derived in the Appendix as the basis of a computer program that simulates a given experiment. Numerical tables of (i) the electron-energy distribution, (ii) the cross section as a function of energy and angle, and (iii) the ground-state-atom velocity distribution, are supplied to the program. The finite detector resolution and pulse width are also taken into account. A simulation of the results of each experimental run is initially attempted using an isotropic cross section. By computing the ratio of experimental to simulated intensity as a function of $\cos\theta$, we obtain a first approximation to the differential cross section at a particular energy. These cross sections can, in turn, be used in the simulation program to generate another series of MTOF spectra and a second comparison can be made yielding a second approximation. The procedure continues until a satisfactory fit to the data is established, typically after two or three iterations.

Figures 3–5 show typical MTOF spectra. Simulated MTOF spectra are also plotted for comparison.

## IV. DISCUSSION OF RESULTS

We have studied the inelastic electron-helium differential cross section over the energy range 19.82 (threshold for the $2\,^3S$ state) to about 20.4 eV. By staying well below the $2\,^1S_0$ threshold at 20.61 eV, we have eliminated any effects due to contributions from that or higher states. A typical set of MTOF distributions is shown in Figs. 3–5.

As indicated in the Appendix, we generally expect two peaks, one at either extreme of the MTOF distribution. Although the experimental cutoffs are fairly sharp, a certain amount of rounding due to lack of resolution is apparent. As expected, the overall width of the distribution increases with increasing energy. The most striking feature is the dramatic shift in the relative peak heights. This variation is due to strong cross-section variations over the energy range under study.

As seen from Eq. (A8), the inverse times of flight are linear in the cosine of the electron scattering angle, with forward scattering at long times and backward scattering at short times. With this rule in mind, it is qualitatively clear from Figs. 3–5 that backward scattering is favored at energies nearest the 19.82 eV threshold, while at somewhat higher energies, for example at 20.3 eV, forward scattering is strongly favored.

Figure 6 shows this behavior in a quantitative form. This set of curves was extracted from the MTOF distributions of Figs. 3–5 by the method described in Sec. III. The above-mentioned details of the cross-section behavior are clearly seen in these curves. To be stressed is the fact that measurements are *not* made at individual electron scattering angles as is done in traditional scattering experiments. Rather, a single MTOF distribution is used to yield the cross section for *all* electron scattering angles at a given energy.

For purposes of comparison, other experimental determinations of the differential cross section are also plotted on Fig. 6. The data of Andrick *et al.*[9] and Pichou *et al.*[10] were obtained at only four angles over a limited range. Both groups determine the cross section by detection of scattered electrons. Although there is qualitative agreement between our results and those of Andrick *et al.* and of Pichou *et al.*, we disagree in some specifics. As can be seen from Fig. 6, we disagree most notably at 19.9 eV with Andrick *et al.* and with both Andrick

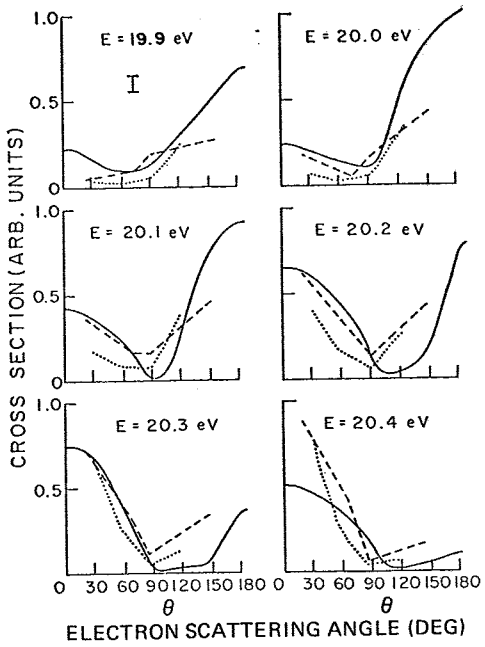


FIG. 6. Differential cross section for excitation of $2\,^3S_1$ helium near threshold. Our results (solid curve, with typical error bar shown on the 19.9 eV curve) are compared to those of Pichou *et al.* (dotted lines connecting their data points) and those of Andrick *et al.* (dashed lines). The values of all experiments are normalized to be the same at 30° for an energy of 20.3 eV.

*et al.* and Pichou *et al.* at 20.3 and 20.4 eV. Convolution of the data of Andrick *et al.* and Pichou *et al.* with our electron-energy distribution has been performed but is not shown since the differences generated are still within our experimental error.

Of particular interest is the cross-section behavior at about 20.2 eV and that near threshold. As can be seen from Fig. 6, our measured differential cross section in the region of 20.2 eV changes from mostly backward to mostly forward scattering, indicating interference between $s$ and $p$ partial-wave contributions. Previous experiments[7-10] have identified this feature as due to the existence of a $p$-wave resonance located in the range 20.2–20.45 eV. The recent high-resolution measurements of the metastable-excitation function by Brunt and his colleagues show this resonance as a broad (0.78 eV) smooth peak centered at 20.27 eV. From our data, we see that the electron scattering changes in a pronounced manner as the electron energy varies in this region. Our most "$p$-like" curve, in the sense of equal forward- and backward-scattering cross sections, is at about 20.2 eV.

Earlier measurements of near-threshold cross-section behavior appeared consistent with isotropic scattering of the electron,[8] and these results appeared to be confirmed by the first MTOF experiments.[17] With our improved resolution and new techniques of data analysis, we find that even at our lowest energy, 19.9 eV, the cross section is already anisotropic. This behavior is consistent with the recent calculations of Nesbet[14] for that energy region. Although he predicts a peak in the $s$-wave partial cross section at 19.89 eV, the $p$-wave contribution is already 30% of that of the $s$-wave. Thus, one would expect to see interference effects already at that low energy. A comparison of the differential cross sections at 19.9 eV given by several investigators is shown in Fig. 7. We also remark that Brunt and his colleagues[3] have identified a break in the excitation function curve at 19.85 eV.

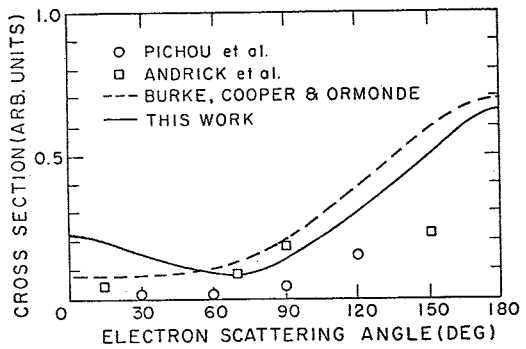


FIG. 7. Differential cross section. Comparison of this experiment (solid curve) with Andrick *et al.* (squares), Pichou *et al.* (circles), and Burke, Cooper, and Ormonde (dashed curve). The Burke, Cooper, and Ormonde curve is normalized to show angular dependence only, while the experimental points are normalized as indicated in Fig. 6.


## ACKNOWLEDGMENTS

We would like to acknowledge useful conversations with Dr. F. Linder, Dr. R. Nesbet, Dr. J. W. Cooper, and Dr. F. H. Read who were kind enough to make available unpublished results. Thanks must also be expressed to Eric Arnold for assistance in the design and construction of electronics, David Crosby for technical assistance, and to Dr. M. Marafi for helpful conversations. This work was supported by the National Science Foundation through Grant No. MPS-74-14593.


## APPENDIX: COLLISION KINEMATICS

We denote the initial and final electron momenta by $\vec{U}_0$ and $\vec{U}$, and the initial and final atom momenta by $\vec{V}_0$ and $\vec{V}$. The conservation of momentum in the collision is then expressed by

$$\vec{U}_0 + \vec{V}_0 = \vec{U} + \vec{V}. \tag{A1}$$

As for conservation of energy, the very small electron-to-atom mass ratio allows us to treat the atom as a "momentum sink"; in other words, the energy required to excite the metastable state can be viewed as coming from the kinetic energy of the electron only, so that we may write

$$U^2 = U_0^2 - 2m\epsilon. \tag{A2}$$

Here $\epsilon$ is the excitation energy of the atom, $m$ is the electron mass, and we have taken the atom mass to be unity. Equation (A2) shows that the magnitude (but not the direction) of the outgoing electron momentum is completely determined by the values of $U_0$ and $\epsilon$.

Figure 8 shows a momentum-vector diagram of the collision. If the atomic momenta are drawn with their tails at the origin $O$, the head of $\vec{V}$ must lie on the surface of a sphere of radius $U$ centered at the total momentum point $Q$. Each velocity represented in the incoming atom beam will contribute its own sphere of radius $U$ centered somewhere on the line $b$-$b$. The possible values of $\vec{V}$ are then those whose heads lie inside the cylinder that forms the envelope of this family of spheres. For a given direction of $\vec{V}$, its magnitude is thus constrained to a finite range between two kinematic limits.

We shall specify the direction of $\vec{V}$ by the polar angles $(\alpha,\beta)$ for which $\vec{V}_0$ is the polar axis, and for which the $U_0V_0$-plane defines the zero of the azimuthal angle $\beta$. We fix the angle $\beta$ first, reducing the problem to one in the $V_0V$ plane. The intersection of this plane with the family of spheres yields a family of circles, and it is easily shown that the magnitudes of the projected vectors $\vec{U}_0'$ and

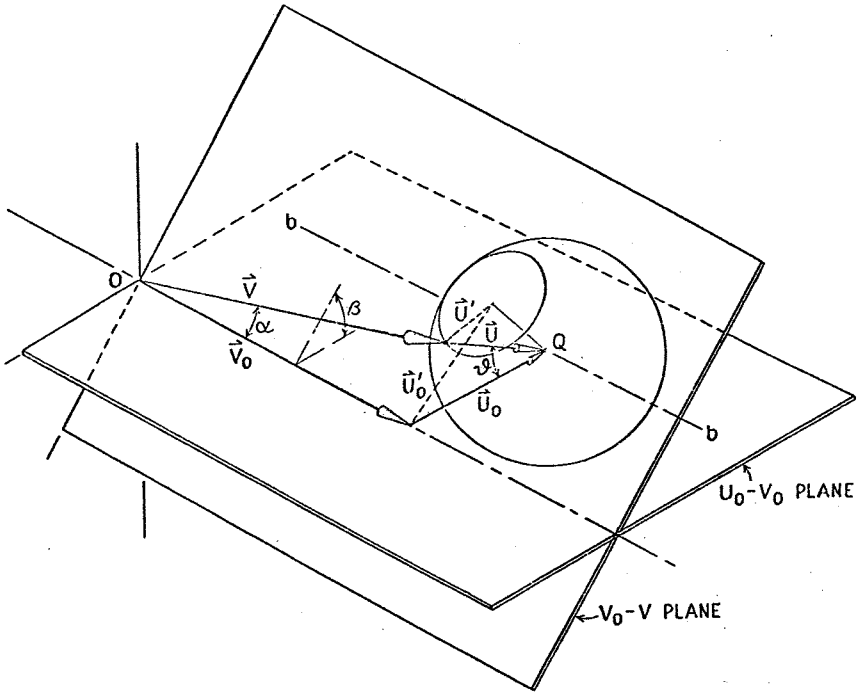


FIG. 8. Momentum diagram of an inelastic electron-atom collision. The momenta of the incoming electron ($\vec{U}_0$) and the incoming atom ($\vec{V}_0$) establish one reference plane; the incoming and outgoing atom momenta ($\vec{V}_0$ and $\vec{V}$) establish the other reference plane. $\vec{U}_0'$ and $\vec{U}'$ are the projections of $\vec{U}_0$ and $\vec{U}$, respectively, on the $V_0V$ plane. Since the magnitude, but not the direction, of $\vec{U}$ is determined by the initial conditions, $\vec{V}$ will terminate somewhere on a sphere (the radius of which is $U$) that is centered about the total momentum point $Q$. If there is a distribution of incoming-atom momenta $f(V_0)$, there will be a continuous series of such spheres with their centers on line $b$–$b$ in the $U_0V_0$ plane.

$\vec{U}'$ are given by

$$U_0' = U_0 \cos\beta \,, \tag{A3}$$

$$U' = (U^2 - U_0^2 \sin^2\beta)^{1/2} . \tag{A4}$$

Only the range of ground-state-atom momenta between the limits

$$V_{0\pm} = (U_0' \pm U')\cot\alpha \tag{A5}$$

will contribute to the signal seen by a detector positioned at $\alpha,\beta$; also, the kinematic limits to the *final* atom momentum for a given $\alpha,\beta$ are

$$V_\pm = (U_0' \pm U')\csc\alpha \,. \tag{A6}$$

The conservation of momentum in Fig. 8 is embodied in the two equations

$$V\cos\alpha = V_0 - U'\sin\theta' \,, \tag{A7}$$

$$V\sin\alpha = U_0' - U'\cos\theta' \,, \tag{A8}$$

where $\theta'$ is the angle between $U_0'$ and $U'$. These equations show that at fixed $\alpha,\beta$ a single value of $V$ corresponds to two different values of $V_0$, and vice versa. For a given $V$, the two values of $V_0$ are

$$V_0 = V\cos\alpha \pm U'\sin\theta' \,. \tag{A9}$$

The actual electron scattering angle $\theta$, that is, the angle between $\vec{U}_0$ and $\vec{U}$, is given by the relation

$$\cos\theta = [1 - (U'/U)^2]^{1/2}\sin\beta + (U'/U)\cos\beta\cos\theta' \,. \tag{A10}$$

The velocity distribution $I(V,\alpha,\beta)$ in the metastable beam is determined by

$$I(V,\alpha,\beta)\, dV\, d\omega = K\sigma(\theta) f(V_0)\, dV_0\, d\Omega \,, \tag{A11}$$

where $d\omega$ is an element of solid angle with reference to the direction of $\vec{V}$, $\sigma(\theta)$ is the differential scattering cross section, $f(V_0)$ is the ground-state-atom velocity distribution, $d\Omega$ is an element of solid angle with reference to the outgoing electron direction, that is, the direction of $\vec{U}$, and $K$ contains the appropriate constants of proportionality. It is easily shown that

$$dV_0\, d\Omega = V^2\, dV\, d\omega / U'U\sin\theta' \,; \tag{A12}$$

also, we must sum the contributions of the two values of $V_0$, as given by Eq. (A9). This yields

$$I(V,\alpha,\beta) = K[f(V\cos\alpha - U'\sin\theta') + f(V\cos\alpha + U'\sin\theta')]V^2\sigma(\theta)/UU'\sin\theta' \,. \tag{A13}$$

The right side of this equation contains the variables $U$, $U'$, $\theta$, and $\theta'$ in addition to the ones explicitly indicated on the left side. Assuming, however, that the electron energy is known, $U$ can be computed from Eq. (A2), and $U'$ from Eq. (A4). As for the angle $\theta'$, Eq. (A8) shows that its cosine is a linear function of $V$; indeed, by comparing that formula with Eq. (A6), we see that $\cos\theta'$ varies from +1 at the lower kinematic limit of $V$ to −1 at the upper one. Thus, the factor $\sin\theta'$ in the denominator of Eq. (A13) indicates that $I(V,\alpha,\beta)$ has singularities at the two values of $V$ that correspond to the kinematic limits (A6). For $V$ outside the limits, $I(V,\alpha,\beta)$ is, of course, zero; just inside, it is very large. As for the actual scattering angle $\theta$, its cosine is given by the rather unwieldy expression (A10); this simplifies greatly, however, in the case of in-plane ($\beta=0$) scattering, when $\theta$ and $\theta'$ become the same.

In order to make comparisons with experiment, it is necessary to integrate $I(V,\alpha,\beta)$ over a distribution of electron energies and over the angular acceptance of the detector, which converts the singularities into finite peaks. Moreover, one generally replaces $I(V,\alpha,\beta)$ with a time-of-flight spectrum $J(t,\alpha,\beta)$ by

$$J(t,\alpha,\beta)=(D/t^2)I(D/t,\alpha,\beta)\,, \tag{A14}$$

where $D$ is the distance between collision region and detector. In the event that the ground-state beam is not well collimated, an additional integration must be performed; this case, and a number of others, are discussed in detail in Ref. 21.

---

*Present address: Joint Institute for Laboratory Astrophysics, Univ. of Colorado and Natl. Bur. Stand., Boulder, Colo. 80309.

†Present address: Goddard Space Flight Center, Code 622, Greenbelt, Md. 20771.

[1]L. Sanche and G. J. Schulz, Phys. Rev. A 5, 1672 (1972).

[2]C. E. Kuyatt, J. A. Simpson, and J. A. Mielczarek, Phys. Rev. 138, A385 (1965).

[3]J. N. H. Brunt, G. C. King, and F. H. Read, J. Phys. B 10, 433 (1977).

[4]G. J. Schulz and R. E. Fox, Phys. Rev. 106, 1179 (1957).

[5]F. M. J. Pichanick and J. A. Simpson, Phys. Rev. 168, 64 (1968).

[6]J. N. H. Brunt, G. C. King, and F. H. Read, J. Phys. B 9, 2195 (1976).

[7]H. Ehrhardt and K. Willmann, Z. Phys. 203, 1 (1967).

[8]H. Ehrhardt, L. Langhans, and F. Linder, Z. Phys. 214, 179 (1968).

[9]D. Andrick, L. Langhans, F. Linder, and G. Seng, in *Ninth Conference on the Physics of Electronic and Atom Collisions (Abstracts)*, edited by J. S. Risley and R. Geballe (University of Washington, Seattle, 1975), pp. 833–834; F. Linder (private communication).

[10]F. Pichou, A. Huetz, G. Joyez, M. Landau, and J. Mazeau, J. Phys. B 9, 933 (1976).

[11]G. J. Schulz, Rev. Mod. Phys. 45, 378 (1973).

[12]P. G. Burke, J. W. Cooper, and S. Ormonde, Phys. Rev. 183, 245 (1969).

[13]R. S. Oberoi and R. K. Nesbet, Phys. Rev. A 8, 2969 (1973).

[14]R. K. Nesbet, Phys. Rev. A 12, 444 (1975).

[15]A. L. Sinfailam, J. Phys. B 9, L101 (1976).

[16]A preliminary report of this work was presented in A. G. Zajonc, G. Weinreich, and J. C. Zorn, J. Phys. B 10, L43 (1977).

[17]R. A. Heppner and J. C. Zorn, Phys. Rev. Lett. 33, 1321 (1974).

[18]A. G. Zajonc, Ph.D. thesis (University of Michigan, 1976) (unpublished) (University Microfilms, Ann Arbor, Mich., Order No. DAH 76–27621).

[19]R. E. Collins, B. B. Aubrey, P. N. Eisner, and R. J. Celotta, Rev. Sci. Instrum. 41, 1403 (1970).

[20]D. P. Donnelly, J. C. Pearl, R. A. Heppner, and J. C. Zorn, Rev. Sci. Instrum. 40, 1242 (1969).

[21]J. Pearl, Ph.D. thesis (University of Michigan, 1970) (unpublished) (University Microfilms, Ann Arbor, Mich., Order No. 70–21754).